Coarsening of capillary drops coupled by conduit networks

Henrik B. van Lengerich,[1] Michael J. Vogel,[2] and Paul H. Steen[1,3,*]
[1]*Department of Chemical and Biomolecular Engineering, Cornell University, Ithaca, New York 14853, USA*
[2]*Independent Researcher, Voorhees, New Jersey 08043, USA*
[3]*Center for Applied Mathematics, Cornell University, Ithaca, New York 14853, USA*
(Received 13 September 2010; published 17 December 2010)

A system of n spherical-cap drops, coupled by a network of conduits, coarsens due to surface tension forces. The total interfacial energy drives the fluid through the conduits such that, with time, the volume becomes increasingly localized into fewer large drops. The coarsening rate is predicted heuristically for drops coupled by orthogonal networks, a porous medium, and fractal networks of various dimensions. The predicted coarsening law as it depends upon the type and dimension of network, total number of drops, and initial drop volume is compared against numerical simulations of large n. Additionally, distributions of large drop volumes are obtained using a Lifshitz-Slyozov-Wagner (LSW) model. The predicted distributions are independent of network topology; in contrast, simulation results depend weakly on the network dimension. The heuristic coarsening rate laws are recovered using the LSW model for all but a square network topology.

DOI: 10.1103/PhysRevE.82.066312 PACS number(s): 47.20.Dr, 47.55.D−, 64.90.+b

I. INTRODUCTION

A system of spherical-cap drops coupled by a network of uniform conduits will coarsen as the capillary force causes some drops to gain volume at the expense of others. We consider a system of n drops. Each has contact-line pinned on identical circles of radii B. The pressure P of each drop is related to the volume V through the surface tension σ by the Young-Laplace equation, cf. Fig. 1. The difference in pressure between drops drives the flow through the conduits. This system is dominated by viscous and surface tension forces (small Bond, Weber, and Reynolds number), and the dissipation within the drop is negligible compared to that through the conduits. The system is started close to a state of almost identical superhemispherical drops (referred to as "large" henceforth) and coarsens as some drops become subhemispherical (referred to as "small" henceforth) by giving volume to the remaining large drops. The surface area is a maximum value initially and decreases monotonically until only a single large drop remains [1]. We seek coarsening laws which predict the number of large drops n_ℓ as a function of time.

A simple experiment illustrates capillary coarsening cf. Fig. 2. A 4×6 array of holes is drilled in a plate. The plate is sealed along its outer edges to a reservoir below and the total volume of water in the reservoir and the drops is controlled by a syringe pump. Initially, by pumping with the syringe, 24 drops are caused to protrude to large volumes. Pumping is then stopped, the total volume fixed, and coarsening ensues. The number of large drops decreases, while the distance between large drops and the difference in volumes between large drops increase.

Coarsening of spherical-cap drops has a central role in the strength of adhesion, both before and after grabbing, for a grab-release adhesion device that we have designed and built [2]. This device, inspired by a leaf beetle [3], uses surface tension to grab onto and release from a substrate. The device works on a principle of parallel action; when many large drops of similar sizes are brought close to a substrate they form liquid bridges, and the total adhesion force is the sum of the forces of individual bridges. Before grabbing, coarsening redistributes liquid in the drops which can decrease the number of bridges formed and, thereby, decrease the total initial adhesive force. After grabbing, the bridges may coarsen over longer time scales which also changes the adhesion. Our focus is on drops, but coarsening of bridges can be studied with a similar approach. Another application where coarsening of capillary drops has been utilized is in microfluidic devices where surface tension forces are used to pump fluid through conduits [4]. This method is attractive in the life sciences due to its compatibility with existing technologies [5]. Although we shall discuss a model of the experiment, Fig. 2, our main interest in this paper is capillary coarsening as a prototype for more general coarsening processes [6–9].

A numerical simulation of the coarsening of $n=100$ drops in Fig. 3 shows the volume of each drop as it varies with time. To observe the coarsening rate, we prefer to plot the time course of the number of large drops n_ℓ as a fraction of the total number n (inset, Fig. 3). At the start, as the disturbance grows from the unstable equilibrium, there is a plateau where $n_\ell\sim n$ after which there is a transient $1<n/n_\ell\lesssim4$ until a coarsening regime develops during which time $(n/n_\ell)^\beta\sim t$, with some exceptions to power-law growth, as we shall discuss below. The coarsening exponent β and the constants that make this expression an equality are the focus of this paper. At the end of coarsening, as a single drop emerges to take all the volume and the final equilibrium state is slowly approached, there is another plateau where $n_\ell\to1$. The initial and final plateaus can be studied using standard linear stability analysis, while the transient that leads to the coarsening regime is more complicated; this coarsening regime is our focus. In this paper we will compare numerical simulations to derived scaling laws.

The time to transfer volume depends on the flow rate through the conduits. Suppose the flow rate Q is driven by a

*phs7@cornell.edu

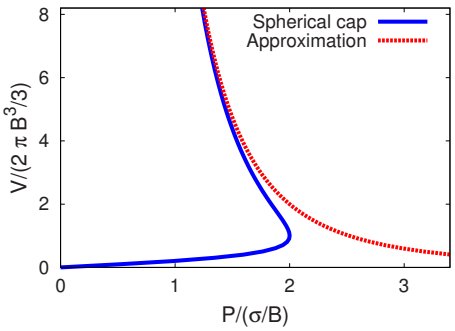

FIG. 1. (Color online) Exact pressure-volume response of a single spherical-cap drop (solid/blue online). Approximate response of a full sphere works well at large volumes (dashed/red online). In this figure only, pressure is scaled by σ/B and volume by $2\pi B^3/3$.

pressure difference ΔP against resistance due to liquid viscosity μ. For a single conduit of hydraulic radius R and length L, $Q \sim R^4 \Delta P/\mu L$ (e.g., Hagen-Poiseuille flow). For a system of two drops coupled through a single conduit and otherwise isolated, the flow rate will change due to changing ΔP since the capillary pressure of the drops varies as volume is drained from the smaller to the larger drop. In the two drop system, ΔP scales as $\sigma/V_0^{1/3}$, where V_0 is the average volume of the drops. When many drops are connected through a network, the relevant driving pressure is that across nearest *large-volume* neighbors ΔP_ℓ. The relevant resistance depends on the network of paths available to move volume between these neighboring large drops and the distance W between large drops. More precisely, the flow rate between the large drops depends (i) on the pressure drop between nearest large neighbors which depends on the extent of coarsening n/n_ℓ through the volume difference of nearest large drops and (ii) on the resistance between large drops which depends on the extent of coarsening through W, and on the network topology though the arrangement of conduits separating large drops. This suggests the following scales, $\Delta P_\ell \sim (\sigma/V_0^{1/3}) h_1(n/n_\ell)$ and $W = L h_2(n/n_\ell)$, where functions h_1 and h_2 of n/n_ℓ are unknown at this stage. For drops connected in a line, it follows that $Q \sim R^4 \Delta P_\ell/\mu W$ and, finally, that a characteristic coarsening time V_0/Q scales as $\mu L V_0^{4/3}/\sigma R^4 h_3(n/n_\ell)$ where h_3 is (yet another) dimensionless function of n/n_ℓ, unknown for now. We may summarize by defining a time scale, useful for all networks considered,

$$T \equiv c \mu L V_0^{4/3}/\sigma R^4. \tag{1}$$

Here, we have added a dimensionless constant c which depends on prescribed network type and dimension. We shall specify c when we specify the network connectivity in Sec. II and this will facilitate the final dimensionless formulation. Closely related to the network of Hagen-Poiseuille conduits is a Darcy porous medium (permeability κ). It turns out that the above time scale is suitable for porous media provided the hydraulic radius is defined through the geometric mean of B^2 and κ, $R^2 \equiv (B^2\kappa)^{1/2}$. The main subject of this paper may now be stated as the determination of the dependence of coarsening time on the dimensionless group n/n_ℓ.

We study two kinds of coupling conduits (Fig. 4). Orthogonal networks (ON) have identical conduits and fractal networks (FN) have conduits of varying length. The unit cell of an ON has a drop at the origin of and conduits aligned along the coordinate axis of a d-dimensional Cartesian space. This unit cell does not repeat forever; the network is bounded. An ON with $d=1$ corresponds to a "linear array," $d=2$ to a "square lattice," and so forth. Here, all but the drops at the boundary are connected to $2d$ other drops. A "completely connected" ON has dimension $d=n-1$ with periodic boundary conditions along each dimension; each drop is directly connected to every other drop twice. FN can take on any fractal dimension d_f by adjusting the ratio of lengths of the conduits. Both d and d_f in these networks are consistent with the "similarity dimension" [10]. We note that the dependence of coarsening rates on the dimension of the sys-

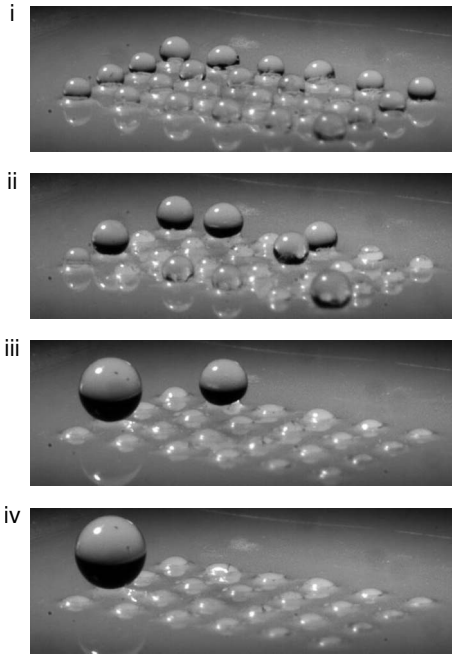

FIG. 2. Coarsening dynamics of a 4×6 array of water drops protruding from 500 μm holes coupled below through a frit with 5 μm pore diameter. Elapsed time i=0 s, ii=2.0 s, iii=21.3 s, iv=31.9 s.

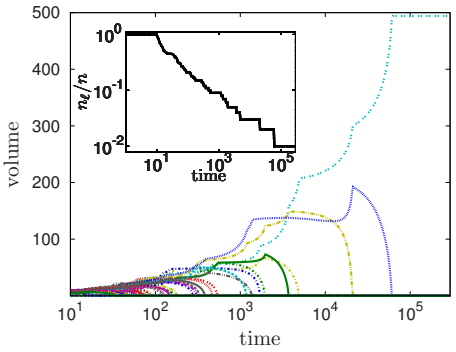

FIG. 3. (Color online) A single numerical simulation of a linear network with 100 drops, where the initial disturbance is randomly chosen from a hypersphere of radius $r_0=0.1$ centered about identical drop volumes of five hemispheres. Inset: n_ℓ/n against time. Volume is in hemispheres, time in scale T_{on}, defined in text.

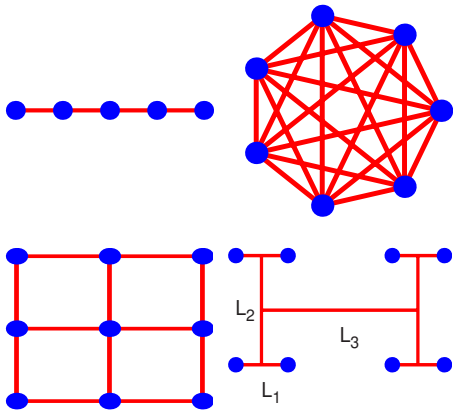

FIG. 4. (Color online) Linear ($d=1$), square ($d=2$), complete ($d=n-1$), and fractal (fractal dimension d_f) networks of conduits connecting drops. Complete network has been flattened from $d=6$, therefore the conduits appear to have unequal lengths; periodic boundary conditions for this network means each line represents two conduits.

tem has been studied in a diverse range of systems (see [11,12], and references therein) but we are not aware of any previous work regarding fractal networks.

The adhesion device design, shown in cross-section in Fig. 5, has a porous medium (PM) adjacent to the top plate to slow the coarsening time. This design consists of a large number of orifices with radii B and center-to-center distances L, below which is a membrane or frit of thickness H_F and Darcy permeability κ_F, and below that is a water reservoir of thickness H_R. Two limiting cases of drop coupling may be identified: (i) flow vertically through the frit and then horizontally through a low-resistance reservoir and (ii) flow only horizontally through the frit. Additionally, fabrication defects can allow drops to communicate through gaps between the frit and the top plate. Scenarios (i) and (ii) are further discussed in the Appendix. We model the coupling of the first case by a complete network. The second case and the coupling through a defect region are modeled with flow through a PM between drops arranged in a linear or square configuration. This study is motivated by the question "can the coarsening exponent distinguish between cases (i) and (ii) (e.g., detect a defect)?."

Classical studies of coarsening of conserved quantities have focused on two types of governing equations. One type

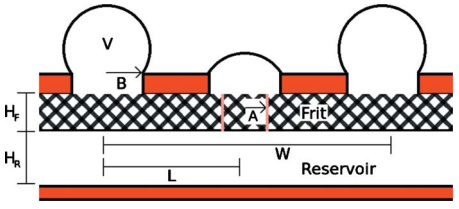

FIG. 5. (Color online) Sketch of adhesion device while coarsening. The height of the frit is H_F; reservoir depth H_R; distance between nearest drops L; and distance between nearest large drops W. For flow horizontal through the a porous media region, the pressure of the drop is applied at a radius A to account for the vertical flow entering from the orifice of radius B.

is a backward heat equation plus a higher-order (usually biharmonic) term, such as the Cahn-Hilliard equation. This equation occurs in application such as spinodal decomposition [6,13] and dewetting of thin films [14,15]. The higher-order term leads to a nonzero most unstable growth rate which determines the early stage of the coarsening into different phases [6,15]. The cluster size of the two phases grow at the late times due to coalescence of clusters [13,14,16,17]. The second type of governing equation is a discretized backward heat equation. This equation is ill-posed in the continuum limit, where the most unstable mode has zero wavelength, but in a system with discrete elements the system can be posed as a set of ordinary differential equations. This type of equation arises in granular mechanics [7,18,19], image enhancement [9], population dynamics [8], as well as the drop coarsening that we study. The methods used to find coarsening rates and size distributions are similar for both partial and ordinary differential equations. Rigorous upper bounds on the decay of energy have been found for both Cahn-Hilliard type equations [20] and discrete backward heat equations [21].

In this work we study orthogonal and fractal networks, both of arbitrary dimension, as formulated in Sec. II. A coarsening law is derived for each of these networks in Sec. III. For networks such as the square, the rates are not simple exponents, and logarithmic terms arise. The coarsening laws are then compared to simulation of the exact equations. The derived laws predict the correct functional relation between pre-exponential factors and the number of drops n, the initial volume, and the size of the disturbance. The distribution of the large drops is predicted in Sec. IV. Although the growth rate of large drops depends on the network, the distribution of the large drops for all networks collapses onto one curve.

II. GOVERNING EQUATIONS

We write three types of governing equations to capture the various conductivities between drops described above. The simplest is an ODE model of drops coupled in orthogonal networks (Fig. 4). Alternatively, a model of drops coupled by a Darcy porous medium is constructed (cf. Fig. 5). This model involves solving a PDE, but we will show in Sec. III that the coarsening law is identical to that for the network of orthogonal conduits. Finally, we consider a fractal network (cf. Fig. 4) where by changing the lengths of the conduits, one can achieve a range of coarsening exponents.

A. Orthogonal networks

Consider a system of drops coupled by a d-dimensional network of orthogonal conduits. The change in the volume of drop i is determined by the flow through the conduits connecting it to its adjacent neighbors

$$\dot{v}_i = \frac{1}{2d}\sum_{k}^{2d} q_{k,i} \quad \text{for} \quad i=[1,\ldots,n], \tag{2}$$

where the sum over k denotes the $2d$ nearest neighbors of drop i. The dot is a derivative with respect to time and $q_{k,i}$ denotes the volumetric flow rate from drop k to drop i. All

the variables have been made dimensionless, with scales V_0 for volume, T_{on} for time and $V_0/(2dT_{on})$ for flow rate (see below in this paragraph for definition of T_{on}). The factor of $2d$ has been added so that when the number of connections to drop i is varied through the network dimension d, and the total dimensional flow rate to a drop i is held constant, then the dimensionless variable $q_{k,i}$ also remains constant. We use a no-flux condition at the edges for linear and square networks and use a periodic boundary condition for completely connected networks, as mentioned. For example, for a linear network the sum at the edges is over just one element (rather than two). The flow rate between any two drops is assumed to be a linear function of the pressure drop

$$q_{k,i} = p(v_k) - p(v_i), \tag{3}$$

where the capillary pressure of an average sphere $2\sigma/[3V_0/(4\pi)]^{1/3}$ has been used to scale the pressure. From here on we assume fully developed Hagen-Poissuelle flow so that the flow rate $Q=(\pi/8)R^4(P_k-P_i)/\mu L$. This determines the *time-scale* $T_{on} \equiv c\mu L V_0^{4/3}/\sigma R^4$ where $c=6^{1/3}/(d\pi^{4/3})$, consistent with Eq. (1). Combining Eqs. (2) and (3) gives a set of ordinary differential equations for the volume of the drops

$$\dot{v}_i = -p(v_i) + \frac{1}{2d}\sum_k^{2d} p(v_k), \tag{4a}$$

with corresponding initial conditions

$$v_i(t=0) = 1 + \epsilon_i/v_0, \tag{4b}$$

where k denotes drops adjacent to i, v_0 is scaled by a hemisphere $2\pi B^3/3$, and ϵ_i is an n-dimensional vector assigning to each drop a randomly chosen volume (in hemispheres) from the surface of an n-dimensional hypersphere of radius $r_0=\sqrt{\Sigma\epsilon_i^2}$ with the constraint $\Sigma\epsilon_i=0$. Simulations of Eqs. (4) use the exact pressure behavior of spherical-cap drops (c.f. Fig. 1), available in closed form. Note that the length scale B enters the scaling only through the initial conditions [Eq. (4b)] and since the initial conditions have "washed out" by the coarsening regime, the coarsening rate is independent of B, contrary to the case for porous media, described next.

B. Porous media

Consider a system of drops protruding from a d-dimensional surface, arranged in an orthogonal grid, with the drops coupled through a Darcy porous medium below the surface (cf. Fig. 5). Recall that the Darcy's law has the fluid velocity proportional to pressure gradient with a coefficient κ/μ, where κ is the Darcy permeability of the porous medium and μ the fluid viscosity. Scaling the typical flow velocity by flow through the orifice, $V_0/(\pi B^2 T_{pm})$, time by T_{pm}, pressure by $2\sigma/[3V_0/(4\pi)]^{1/3}$, and L for the gradient length scale, the dimensionless Darcy's law becomes

$$u = -\nabla p, \tag{5}$$

provided the time-scale $T_{pm} \equiv c\mu L V_0^{4/3}/B^2\kappa\sigma$ is chosen with $c=3^{1/3}/(2^{5/3}\pi^{4/3})$. This reconciles with Eq. (1) for $R^4=B^2\kappa$. Inserting Darcy's law into the continuity equation gives

$$0 = \nabla^2 p. \tag{6}$$

The boundary conditions to this equation are determined by the pressures of each of the drops. The pressure of a drop $p(v_i)$ is specified at a dimensionless "cutoff" radius $a \equiv A/L$ from the center of the base of drop i, to account for the finite orifice area πB^2 where the drop joins the frit (cf. Fig. 5). This cutoff distance scales with the orifice radius $A \sim B$. To simplify the formulation we assume the flow through the frit happens in the same number of dimensions as the arrangement of drops. Therefore, the spherical hypershell at which the pressure is applied is $d-1$-dimensional, consistent with the Laplacian in Eq. (6) which is d-dimensional. The evolution the volume of drop i can be obtained by a balance of a shell of radius a to give

$$\dot{v}_i = -\int_{\Omega_i} u \cdot n_i ds, \tag{7}$$

where the surface Ω_i of radius a and normal vector n_i depend on d. The dimensionless surface area Ω_i is scaled by the orifice area πB^2. Once the volume of the drops are specified, the pressure field can be solved using Eq. (6) and the volumes can be iterated using Eq. (7). The initial condition can be specified in terms of drop volumes, as in Eq. (4b).

C. Fractal networks

We formulate the governing equations for a system of $n=2^{s_n}$ drops arranged in a fractal configuration (for $s_n=3$, see Fig. 4). The length of the shortest conduits is L_1, the length of conduits that connects the midpoints of two L_1 segments is L_2, and so on for all s_n lengths. The lengths are scaled by the shortest length $l_i=L_i/L_1$, thus $l_1=1$. The governing equations are constructed by first writing a balance equation on the volume of all n drops assuming we know the pressures $[p_a,p_b,\ldots]$ at the intersection of the l_1 and l_2 conduits. For example

$$\begin{aligned} \dot{v}_1 &= \frac{2}{l_1}(p_a - p_1), \\ \dot{v}_2 &= \frac{2}{l_1}(p_a - p_2), \\ &\vdots \end{aligned} \tag{8}$$

Scales for volume, pressure, and volumetric flow rate are the same as for orthogonal networks. Each drop is connected to only one conduit, therefore the time scale corresponds to that of the ON with $d=1/2$. The time-scale $T_{fn} \equiv c\mu L_1 V_0^{4/3}/\sigma R^4$ with $c=2\times 6^{1/3}/\pi^{4/3}$ results.

To determine the pressures at the intersections $[p_a,p_b,\ldots]$ we write a volume balance around all the intersections of conduits of length l_1 and l_2. For example, a balance about the midpoint of drops 1 and 2 gives

$$0 = \frac{2}{l_1}(p_1 - p_a + p_2 - p_a) + \frac{2}{l_2}(p_b - p_a), \tag{9}$$

where p_b is the pressure at the midpoint of the conduit of length l_2 connecting the conduit of length l_1 from above, to

another conduit of length l_1. Balances of the form of Eq. (9) are written with a recursive code for all $n-2$ intersections, giving $n-2$ equations for $n-2$ unknown intersection pressures. By solving for all intersection pressures in terms of drop pressures we obtain a system of n equation for the dynamics of the drops,

$$\dot{v}_i = \sum_{j=1}^{n} c_{ij}(p_i - p_j), \tag{10a}$$

$$v_i(t=0) = 1 + \epsilon_i/v_0, \tag{10b}$$

where c_{ij} is the adjacency matrix of the conduit network and ϵ_i and v_0 are as for orthogonal networks. Numerical simulation of Eqs. (10), like Eqs. (4), uses the exact pressure relation of spherical-cap drops (c.f. Fig. 1). To obtain self-similar networks, we set the lengths of the conduits as

$$l_1 = 1,$$

$$l_i = \omega^{i-2}(\omega - 1) \quad \text{for} \quad 2 \le i \le s_n, \tag{11}$$

where $\omega \ge 1$. When one drop is eliminated from the end of each conduit of length l_1, the system can be rescaled by ω and overlaid on half the original image. This elimination of half the large drops and rescaling by ω can be done for all s_n lengths. Therefore [10], the fractal dimension is

$$d_f \equiv \log(2)/\log(\omega). \tag{12}$$

This dimension (the "similarity dimension") can be used to recover the dimension d of the ON [10].

III. COARSENING RATES: HEURISTIC PREDICTIONS AND SIMULATION RESULTS

A heuristic argument can be made to find the number of large drops as a function of time. To do this, we write an equation for the evolution of a typical growing large drop at some intermediate time. We assume the large drops are evenly distributed in space because any more closely spaced large drops will more quickly coarsen due to the lower resistance between them. A typical large drop will be connected to other large drops a dimensionless distance $w \equiv W/L$ away. Small drops cannot become large as no drop can have more pressure than a hemisphere. Therefore, the majority of the flow transferred to a (growing) large drop must originate from another (shrinking) large drop. We can solve for the pressure profile below the small drops to calculate the resistance to flow between large drops. The coarsening rate will depend on the network resistance through w and on the network connectivity.

A. Orthogonal networks: Large drop growth

The resistance between two large drops in an orthogonal network will be determined by the flow through a network of conduits below the small drops (since small drop growth is negligible, $\dot{v}_s \approx 0$). Substituting this into Eq. (4a) gives a standard discretized version of the Laplace equation which, for large w, takes the continuum form,

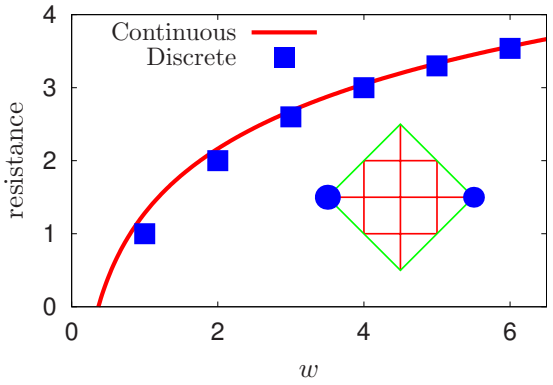

FIG. 6. (Color online) Network resistance for flow between two drops in square network: continuous (solid) vs discrete (squares) resistance. The continuous curve is fit to the discrete curve with a value of $\ln(a) = -1.7$. Inset: diamond-shaped domain through which flow travels for $w=4$.

$$0 = \nabla^2 p. \tag{13}$$

For linear networks, this approximation is true for all w since the solution to Laplace's equation is identical to that for discrete resistors in series. For square networks, a comparison against discrete resistors shows that it also works well down to very small w (Fig. 6).

Next, we solve Eq. (13) in radial coordinates with one drop at the origin and $2d$ drops at a distance w. The boundary condition for the drop at the origin is $p(r=a)=p_\ell$. The pressure at the nearest-neighbor large drops at a distance w is set to the mean-field pressure p^*. Therefore the pressure at the surface of the disk of radius $w/2$ is $p(r=w/2)=(p^*+p_\ell)/2$. Applying these boundary conditions we obtain

$$p = \frac{1}{2}\frac{p_\ell - p^*}{a^{2-d} - (w/2)^{2-d}}(r^{2-d} - a^{2-d}) + p_\ell \quad \text{for} \quad d \ne 2, \tag{14a}$$

$$p = \frac{1}{2}\frac{p_\ell - p^*}{\ln(a) - \ln(w/2)}[\ln(r) - \ln(a)] + p_\ell \quad \text{for} \quad d = 2. \tag{14b}$$

Evaluating this expression at the location of the nearest-neighbor drops ($r=1$) and inserting this into the dynamical system for the orthogonal networks [Eq. (4a)] gives

$$\dot{v}_\ell = \frac{1}{2}\frac{p_\ell - p^*}{a^{2-d} - (w/2)^{2-d}}(1 - a^{2-d}) \quad \text{for} \quad d \ne 2, \tag{15a}$$

$$\dot{v}_\ell = -\frac{1}{2}\frac{p_\ell - p^*}{\ln(a) - \ln(w/2)}\ln(a) \quad \text{for} \quad d = 2. \tag{15b}$$

In the limit $a \ll 1$, growth of large drops is given by

$$\dot{v}_\ell = \frac{p^* - p_\ell}{2(w/2)^{2-d}} \quad \text{for} \quad d = 1, \tag{16a}$$

$$\dot{v}_\ell = \frac{p^* - p_\ell}{2} \quad \text{for} \quad d \geq 2. \tag{16b}$$

For $d=1$, the resistance between drops of a distance w is equal to w, as the resistors add in series. From Eq. (15a) we see that this corresponds to $a=0$. For $d>2$, a is negligible for a different reason. There, the exponent on a makes the equations in the limit of small a more accurate. For $d=2$ the approximation is least valid, and therefore, we will leave a in the prediction of these coarsening rates. The value of a is determined by comparing the resistance through a diamond-shaped domain to the resistance given by Eq. (15b), cf. Fig. 6. A value of $\ln(a)=-1.7$ is found as a best fit to match the resistance in a continuous porous medium with a discrete network model.

B. Porous medium: Large drop growth

For the porous medium, start by noting that Eq. (13) also governs the pressure in porous media [c.f. Eq. (6)]. Applying the same boundary conditions as for the orthogonal networks leads to the same solutions, Eqs. (14), for the pressures. We then insert the pressure profiles [Eqs. (14)] into Eqs. (5) and (7) and observe that, by rescaling the time with scales,

$$T^*_{pm} \equiv T_{pm} \frac{1 - a^{2-d}}{(2-d)\int_{\Omega(r=1)} ds} \quad \text{for} \quad d \neq 2, \tag{17a}$$

$$T^*_{pm} \equiv T_{pm} \frac{-\ln(a)}{\int_{\Omega(r=1)} ds} \quad \text{for} \quad d = 2, \tag{17b}$$

one arrives at Eqs. (15). Here, the subscript on the integral indicates the radius of the surface is unity. In summary, the equations for the growth of large drops are the same for the porous medium and orthogonal networks. The main difference is that, for networks, a is a fixed quantity and, for porous media, it is a material parameter that depends on the ratio of B/L as well as the exact experimental setup. The close relationship between ON and PM has been anticipated by [22], among others [23]. It is included here for completeness and because of its relevance to the motivating application. The pressure in hexagonal, triangular, and other regular networks are also determined by a d dimensional Laplace equation (cf. [22]); the dynamics of drops on these networks are equivalent to those on ON and PM modulo a change in the time scale.

C. Orthogonal networks and porous media: Prediction and simulation

We can now calculate the coarsening rates from Eqs. (15b), (16a), and (16b) (for $d>2$). The majority of the volume is in the large drops and the total volume of the system is constant, therefore

$$v_\ell n_\ell \approx n, \tag{18}$$

regardless of network topology. For all large drops the pressure can be approximated as

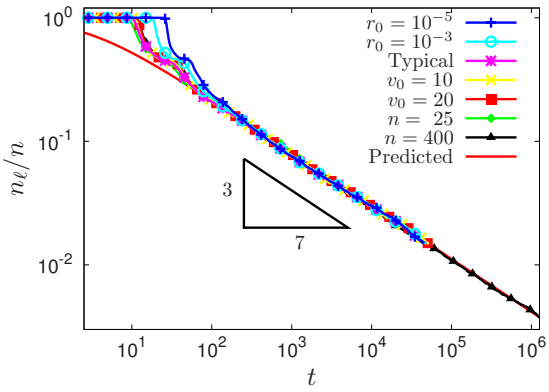

FIG. 7. (Color online) Coarsening of linear network according to Eq. (21). Simulations for $n=100$, $r_0=0.1$, and $v_0=5$ (typical), unless otherwise noted in legend. Each simulation curve is an average of 100 simulations each with random initial condition. Simulations are cut off before they reached steady state for presentation purposes.

$$p_\ell \approx v_\ell^{-1/3}, \tag{19}$$

which is the pressure of a sphere. This approximation is more accurate for larger volumes, as shown in Fig. 1. The large drops dominate the dynamics, therefore the mean-field pressure should depend on the pressure of the large drops. For simplicity we choose the mean field pressure to be directly proportional to the pressure of the large drop

$$p^* = (1 + \delta) p_\ell, \tag{20}$$

where δ is undetermined.

For linear networks ($d=1$), after turning "approximate" relationships into "equality," we insert Eqs. (18)–(20) as well as a relation between the distance of large drops $w \approx n/n_\ell \approx v_\ell$ into Eq. (16a) and integrate to give

$$\left(\frac{n}{n_\ell}\right)^{7/3} - 1 = \frac{7}{3}\delta t. \tag{21}$$

The lower bound of integration has a negligible effect and was chosen to be zero for convenience. This coarsening law not only gives us the time it takes for small drops to coarsen, it also includes the dependence on the total number of drops, and shows no dependence on initial disturbance size and initial volume. These dependencies are verified against numerical simulations of Eq. (4) shown in Fig. 7. The value of the mean-field pressure determines the intercept in the coarsening plot; a value of $\delta=0.15$ was used to match the simulation results. The value of δ did not need to be adjusted when r_0, v_0, or n was varied.

Numerical integration of Eq. (4) (cf. Fig. 7) show that the initial coarsening rate is slower, and then faster, than that which is predicted. For smaller disturbances, the time until the first large drop becomes small increases. As the size of the disturbance r_0 decreases the initial condition is getting closer to an unstable fixed point, therefore it takes longer to escape the neighborhood of the fixed point and start to coarsen. Once the first drop becomes small, many others quickly follow. The validity of the heuristic coarsening law

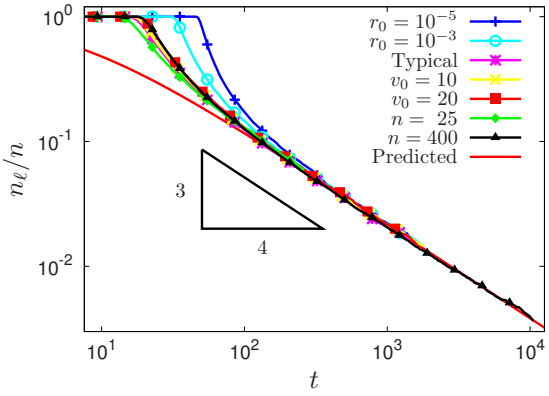

FIG. 8. (Color online) Coarsening of complete network according to Eq. (22). Simulations for $n=100$, $r_0=0.1$, and $v_0=5$ (typical), unless noted in legend. Each simulation curve is an average of 100 simulations each with random initial condition. Simulations are cutoff before they reached steady state for presentation purposes.

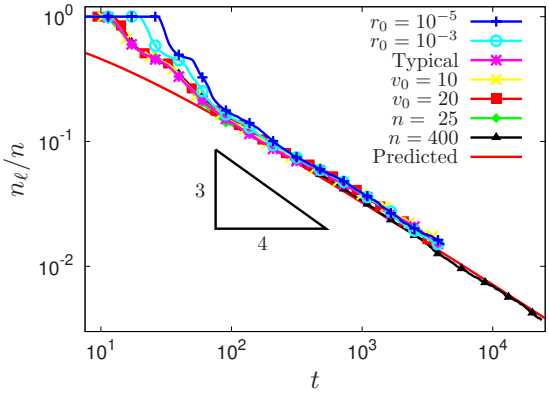

FIG. 9. (Color online) Coarsening of square network ($d=2$) according to Eq. (23). Simulations for $n=100$, $r_0=0.1$, and $v_0=5$ (typical), unless noted in legend. The predicted coarsening rate does not have a $-3/4$ exponent due to the nonzero value of a.

at early times is related to the distribution of large drop volumes, discussed in Sec. IV. The initial time is exaggerated by the log scale; discrepancies between the theory and experiment at initial times have a negligible effect on the long-time coarsening.

We do not observe any effects from the finite size of the network. As the number of drops is increased, a smaller fraction of drops are affected by the boundaries, however, the numerical data collapses onto a single curve for the three values of n simulated.

For orthogonal networks where $d>2$ and $a \ll 1$ we insert Eqs. (18)–(20) into Eq. (16b) and integrate to obtain

$$\left(\frac{n}{n_\ell}\right)^{4/3} - 1 = \frac{2}{3}\delta t. \tag{22}$$

This coarsening law is compared against simulations of Eq. (4) for the completely connected network in Fig. 8. By including the dimension d in the time scale, the simulations collapse using n_ℓ/n even though the number of connections per drop increases with n since $d=n-1$ for the complete network.

For square networks ($d=2$) where a is not negligible, we insert Eqs. (18)–(20) as well as the relation $w^2 \approx n/n_\ell \approx v_\ell$ into Eq. (15b) and integrate to obtain

$$\left[\left(\frac{n}{n_\ell}\right)^{4/3} - 1\right]\left[\frac{3}{4} + 2\ln(2a)\right] - \left(\frac{n}{n_\ell}\right)^{4/3}\ln\left(\frac{n}{n_\ell}\right) = \frac{4\ln(a)}{3}t, \tag{23}$$

where the value of a, mentioned previously, is given by $\ln(a)=-1.7$.

The derived coarsening law for the square network [Eq. (23)] matches the simulations of Eq. (4) as can be seen in Fig. 9. The difference between the $-3/4$ coarsening law, which would be obtained in the limit of $a \to 0$, and the coarsening law including logarithmic terms due to finite a [Eq. (23)] can also be seen in Fig. 9.

D. Fractal network: Prediction and simulation

In the fractal network the $n/2$ pairs of drops closest to each other will coarsen first because the resistance between them is the lowest. In the next stage of the process (denoted $s_i=2$) the $n/4$ pairs of drops next closest to each other coarsen, and this process continues until only one drop is left. We neglect the pressure of the small drops, since the flow between the larger drops does not pass below these. The total resistance between drops depends only on the length between the remaining large drops, which goes as $\Sigma_{j=1}^{s_i} l_j = (2^{s_i})^\lambda$, where $\lambda \equiv 1/d_f$ and the stage s_i is given by $s_i = \log_2(n/n_\ell)$. The growth rate of a large drop goes as

$$\dot{v}_\ell = \frac{p^* - p_\ell}{\sum_{i=1}^{s_n} l_i} = \frac{p^* - p_\ell}{v_\ell^\lambda}. \tag{24}$$

Inserting the approximation for the pressure [Eq. (19)], the mean-field pressure [Eq. (20)], and the conservation of volume [Eq. (18)], and then integrating gives the coarsening law

$$\left(\frac{n}{n_\ell}\right)^{4/3+1/d_f} - 1 = (4/3 + 1/d_f)\,\delta t. \tag{25}$$

Comparison of Eq. (25) against simulations of fractal systems Eq. (10) is shown in Fig. 10. The pre-exponential factor in the coarsening law was chosen as $\delta=1/4$, and this fit matched the numerical simulations for $d_f=1/2,1,2$, and 70; however, for small dimensional systems a range of fitting factors could have been justified. As seen in Eq. (25), *systems can be created with any coarsening exponent between* $-3/4$ and 0 *by changing the fractal dimension of the network*. In Fig. 10 the simulations show a "staircasing" behavior due to the coarsening stages. Each step in the staircase halves the number of large drops. Staircasing is more prominent at smaller dimensions where the resistance, and therefore also the time, between the s_i and s_{i+1} stages is larger. For $d_f=1$ the system coarsens at the same rate as that for the linear networks. For $d_f=2$ the drops coarsen as $n_\ell \sim t^{-6/11}$ in contrast to the square coarsening rate of $n_\ell \sim t^{-3/4}$ plus logarithmic terms. This was verified by numerical simulations

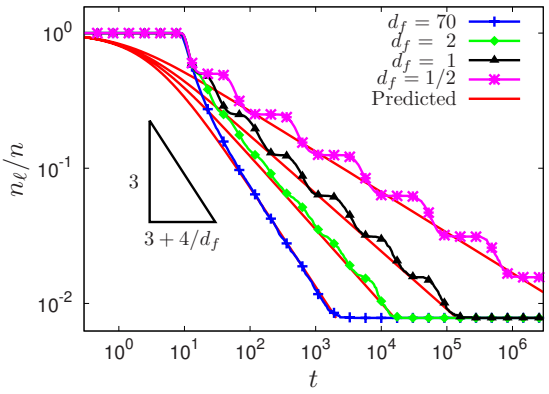

FIG. 10. (Color online) Coarsening of fractal network (various d_f). Simulations for $n=128$, $v_0=5$, and $r_0=0.1$. Simulations are averaged over 100 random initial conditions. Predictions according to Eq. (25).

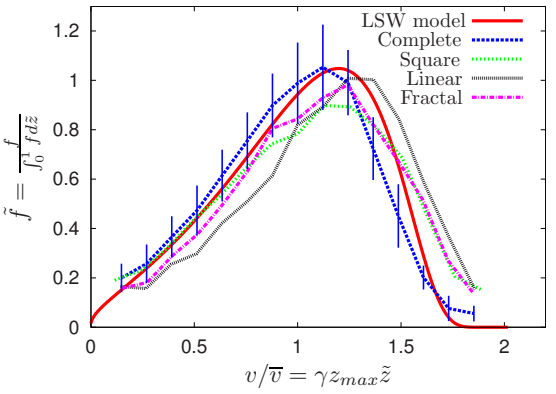

FIG. 11. (Color online) Probability distribution of large drop volumes. Simulations of complete, square and linear networks done with 2500 drops, Fractal network ($d_f=2$) with 2048 drops. Only data between $500 > n_\ell > 200$ is used. All simulations had an initial volume of $v_0=5$ and a perturbation size of $r_0=0.1$. One standard deviation for the completely connected network is shown; error for other networks is of similar magnitude.

and is shown in Fig. 10. The coarsening rate $n_\ell \sim t^{-6/11}$ would be obtained in the square network only if the resistance between large drops would be proportional to w instead of $\ln(w)$. The coarsening for orthogonal networks is quicker than that for fractal networks for $1 < d_f < \infty$. In orthogonal networks the resistance between large drops is lower due to the multiple flow paths in parallel, whereas the resistances add in series for the fractal networks. In the limit $\omega \to 1$ the infinite dimensional fractal network becomes identical to the completely connected network to within a constant scaling factor of time; simulations and predictions confirm this limiting behavior.

IV. DISTRIBUTION OF LARGE DROP VOLUMES AND SELF-SIMILAR COARSENING RATES

To determine the difference between the large drop volumes throughout the coarsening we seek a self-similar distribution of the large drop volumes. From the distribution some of the heuristic coarsening laws from the previous section can be recovered. We follow the formulation presented by Gratton and Witelski [24] to apply the Lifshitz-Slyozov-Wagner (LSW) [25,26] model to our system of drops. It is assumed that the system has coarsened for long enough so that the initial perturbation has evolved into a self-similar distribution of volumes, but not so long that the number of large drops is too few to justify a continuous distribution. We write a conservation law of the number density of large drops ϕ as

$$\frac{\partial \phi}{\partial t} + \frac{\partial}{\partial v}(\phi \dot{v}) = 0, \tag{26}$$

where $\dot{v}$ is given by Eqs. (16a) and (16b), or (24) for linear networks, orthogonal networks where $d \geq 2$ and $a \to 0$, or fractal networks, respectively. We can integrate the number distribution to obtain the number of large drops, the average large drop volume or the average large drop pressure

$$n_\ell = \int_0^\infty \phi dv, \tag{27}$$

$$\bar{v} = \frac{1}{n_\ell} \int_0^\infty v \phi dv, \tag{28}$$

$$\bar{p} = \frac{1}{n_\ell} \int_0^\infty v^{-1/3} \phi dv. \tag{29}$$

We construct a similarity variable $z \equiv v/v^*$ where v^* is a mean-field volume and seek a self-similar solution of the form

$$\phi = t^{-\alpha} f(z). \tag{30}$$

We assume the mean-field volume scales as $v^* = \nu t^\beta$ and the relation between the mean-field volume and average volume is given by $\gamma = v^*/\bar{v}$. The value of the pressure is given by Eq. (19), thus the mean-field pressure is $p^* = (v^*)^{-1/3}$, where α, β, γ, and ν are undetermined coefficients. In the equations for $\dot{v}$ we use the mean volume to determine the distance to the nearest large drops, as a result the function f will be independent of the network. Using the conservation of volume in large drops $n = \int_0^\infty v \phi dv$ we find the relation $\alpha = 2\beta$. From Eq. (26) we find the value of α and an ordinary differential equation for the function f

$$\frac{df}{d\tilde{z}} = \frac{2\tilde{z}^{4/3} - 1}{-\tilde{z}^{7/3} + 4\tilde{z}^{4/3} - 3\tilde{z}} f, \tag{31}$$

where $\tilde{z} \equiv z/z_{max}$. The undetermined coefficients β and z_{max} are found by setting the denominator of Eq. (31) and its derivative to zero, see [11,24,25] for details. The value of γ can be found from its definition. The values $z_{max}^{1/3} = 4/3$ and $\gamma = \int_0^1 f d\tilde{z} / (z_{max} \int_0^1 \tilde{z} f d\tilde{z}) \approx 0.8509$ were found. We integrate Eq. (31) numerically and compare this to the distributions of large drops for various networks from simulations of Eq. (4) in Fig. 11.

The probability distributions for the smaller dimensional networks are shifted to higher probabilities of larger volume drops, according to Fig. 11. The complete network most ac-

TABLE I. Comparison of heuristic and LSW coarsening rates as well as δ values used to fit the data for orthogonal networks, porous media, and fractal networks. LSW predicts a pre-exponential factor of $\delta=3^3/4^4\approx 0.105$ for all networks.

Network	Dimension	Heuristics	Simulation δ	LSW
Linear ON	$d=1$	$(\frac{n}{n_\ell})^{7/3}-1=\frac{7}{3}\delta t$	0.15	$(\frac{n}{n_\ell})^{7/3}=\frac{7}{3}\frac{3^3}{4^4}t$
Square ON	$d=2$	$[(\frac{n}{n_\ell})^{4/3}-1][\frac{3}{4}+2\ln(2a)]-(\frac{n}{n_\ell})^{4/3}\ln(\frac{n}{n_\ell})=\frac{4\ln(a)}{3}t$	0.20	NA
ON $a\to 0$	$d\geq 2$	$(\frac{n}{n_\ell})^{4/3}-1=\frac{2}{3}\delta t$	NA	$(\frac{n}{n_\ell})^{4/3}=\frac{2}{3}\frac{3^3}{4^4}t$
Complete ON	$d=n-1$	$(\frac{n}{n_\ell})^{4/3}-1=\frac{2}{3}\delta t$	0.25	$(\frac{n}{n_\ell})^{4/3}=\frac{2}{3}\frac{3^3}{4^4}t$
Porous media		Same as above		
Fractal	$0<d_f<\infty$	$(\frac{n}{n_\ell})^{4/3+1/d_f}-1=(\frac{4}{3}+\frac{1}{d_f})\delta t$	0.25	$(\frac{n}{n_\ell})^{4/3+1/d_f}=(\frac{4}{3}+\frac{1}{d_f})\frac{3^3}{4^4}t$

curately matches the predicted probability distribution. Fractal networks of $d_f<1$ do not reach a self-similar volume distribution. These low-dimensional systems have very prominent stepping behavior, as seen in Fig. 10, and therefore the exact time at which the probability distribution is evaluated (on the flat or on the steep part of the step) can yield very different results. It was observed that, when the numerical simulations are given initial conditions that match the self-similar large volume distribution, they follow the heuristic coarsening laws even at early times. The self-similar distributions are apparently stable distributions.

The coarsening law can be found from Eq. (27) for regular networks where $a\to 0$ and fractal networks, using the values of γ and α found previously. The results are shown in Table I. The coarsening exponents and the dependence on the total number of drops and initial volumes compare favorably to those found by heuristics. For $d=2$ and $a>0$, the coarsening law is a transcendental function of t and therefore cannot be expected from a similarity solution of the form Eq. (30). The LSW model also predicts a pre-exponential factor to be compared to a fit value of the heuristics. The probability distribution of large drops predicted by the LSW model is independent of network topology; therefore, the pre-exponential factor predicted is also independent of network topology. The LSW model predicts $\delta=3^3/4^4\approx 0.105$, which is most accurate for low-dimensional systems.

V. DISCUSSION AND SUMMARY

Simulations of coarsening behavior of a system of spherical-cap drops obtained by solving the "exact" equations are reported. Drops are connected by conduits laid out in orthogonal and fractal networks with network size n, initial conditions, and system dimensions (d and d_f) varied in the simulations. Scaling-law predictions are derived by presuming dominant balances (heuristics) for coarsening growth and by assuming the LSW model for size-distribution dynamics. Table I summarizes the predictions. Figures 7–10 compare simulation of coarsening rates against prediction. Figure 11 compares simulation of distribution of size against prediction of the LSW model.

For coarsening rates, the prediction captures the dependence on initial total volume, initial drop size distribution, and network size with a single fitting parameter for each network type (Table I). The initial volume dependence is accounted for by the time scale, and enters only through the perturbation size of the initial condition. The initial drop distribution is "washed away" as the large drop distribution converges to the self-similar distribution shown in Fig. 11. The network size enters the coarsening rate only as a ratio through the volume balance $v_\ell\approx n/n_\ell$. Coarsening depends most strongly on the dimension of the network. The coarsening exponent increases from 3/7 to 3/4 going from $d=1$ (linear ON) to $d=2$ (square ON, $a\to 0$) dimensions, as anticipated [21]. For $d>2$ the exponent remains at 3/4 while coarsening continues to increase but in a linear fashion, as reflected in the time-constant dependence on d (Table II). The complete ON are optimally connected and show a maximum coarsening rate for any chosen n, among all the ON networks. Effects of the cutoff distance a at which the pressure of the drop is applied play the strongest role in planar networks $d=2$ where logarithmic corrections to the power law growth must be included to capture the simulations (Fig. 9).

The fractal network is distinguished by drops with exactly one nearest neighbor (a pairwise competition occurs between drops at each stage) but a resistance from stage to stage that changes in a self-similar fashion. Putting $d_f=1$ corresponds to resistances that increase in a geometric fashion and yields a coarsening rate that is identical to the linear ON. Increasing to $d_f=\infty$, the FN coarsens with the same power law as the complete ON but with a different constant in the time scale. For all other d_f, the FN coarsens slower than the ON because the resistance of many conduits in series is greater than that for conduits in parallel.

Drops coupled by a two-dimensional porous medium coarsen with the same exponential behavior as those coupled

TABLE II. Time scales for orthogonal networks, porous media, and fractal networks.

Connectivity	Time scale (T)	Constant (c)
ON	$c\mu LV_0^{4/3}/\sigma R^4$	$6^{1/3}/(d\pi^{4/3})$
PM $d\neq 2$	$c\mu LV_0^{4/3}/B^2\kappa\sigma$	$\frac{3^{1/3}(1-a^{2-d})}{2^{5/3}\pi^{4/3}(2-d)\int_{\Omega(r=1)}ds}$
PM $d=2$	$c\mu LV_0^{4/3}/B^2\kappa\sigma$	$\frac{-3^{1/3}\ln(a)}{2^{5/3}\pi^{4/3}\int_{\Omega(r=1)}ds}$
FN	$c\mu L_1V_0^{4/3}/\sigma R^4$	$2\times 6^{1/3}/\pi^{4/3}$

by complete networks, cf. Table I. Hence, a measured exponent alone cannot distinguish if the flow is through the reservoir, frit, or a defect region; that is, cannot distinguish between cases (i) and (ii) above. For linear arrays of drops the coarsening exponent changes significantly from linear to complete coupling. In two-dimensional arrays different flow types might be distinguishable by the coarsening time, provided the time scales differ significantly.

In some instances the practitioner may find it convenient to know the actual times the system might take to reach certain milestones, such as half-coarsening ($n_L=n/2$) or full-coarsening ($n_L=1$). Expressions for these times can be readily derived from Tables I and II. Due to the appearance of d in the time scale for orthogonal networks, changing the number of drops will change the time scale for the complete network ($d=n-1$), but not for other networks. That is, with R, V_0, L, and fluid properties held constant, the time for half-coarsening is independent of n for square networks; however, it scales as $1/n$ for complete networks. The time for full-coarsening scales as $n^{4/3}$ for square networks, and $n^{1/3}$ for complete networks. In practice, these times can be highly dependent on the initial distribution of imperfections, perhaps making the coarsening exponent a more reliable metric.

For drop size predictions by the LSW model, the pre-exponential factor is found to be independent of the network connectivity. In contrast, the simulations show that the lower dimensional networks have distributions shifted to larger volumes and smaller pre-exponential factors. The differences in large volume distributions cannot be attributed to different initial conditions (cf. [27]), as all initial conditions are picked from the same distribution. The reason the predicted distributions are insensitive to network type is because the mean volume is used to determine the distance to nearest large drops (w). The results suggest that the LSW model could be improved by incorporating the effects of network connectivity through the use of a better estimate of the large drop separation.

ACKNOWLEDGMENTS

H.B.v.L. and P.H.S. would like to acknowledge helpful comments regarding coarsening in porous media from Dejan Slepčev and support of the IMA (University of Minnesota). H.B.v.L. is thankful for helpful correspondence with Micheal Gratton. P.H.S. thanks Bud Homsy and Detlef Lohse for helpful conversations. This work was supported by NSF Grant No. CBET-0653831 and NASA Grant No. NNX09AI83G.

APPENDIX: FLOW TYPES IN ADHESION DEVICE

In the low-resistance reservoir limit (i), the resistance through the reservoir is much less than the resistance to flow vertically through the frit $4\mu W/(H_R^3) \ll 2\mu H_F/(B\kappa)$ which is much less than resistance to flow horizontally through the frit $2\mu H_F/(B\kappa) \ll \mu W/(H_F\kappa)$. The liquid travels from a drop vertically through the frit to the reservoir and then through the frit again to another drop. In this case the resistance between drops is dominated by flow vertically through the frit. The resistance is independent of the distance between drops, therefore this type of flow is modeled as a complete network.

The flow travels only through the frit (ii) when the resistance to flow horizontally through the frit is much less than the resistance through the reservoir $\mu W/(H_F\kappa) \ll 4\mu W/(H_R^3)$ or much less than the resistance vertically through the frit $\mu W/(H_F\kappa) \ll 2\mu H_F/(B\kappa)$. Here, the resistance between drops depends on the distance between drops. Koplik [22] has shown that creeping flow through networks of conduits connecting cavities behaves effectively as flow through a porous medium on the large scale, and this is also true for our system (Sec. III B). For this reason, simulations of this type of flow will be modeled with a linear or square network of conduits.

The experiments can be more complicated than these limiting cases. With a thick frit, flow horizontally through the frit dominates at early times when the large drop distance is less than the thickness of the frit. Thereafter, the flow is dominated by the resistance perpendicular to the frit. A difficulty in fabricating these small-scale devices is ensuring that there are no gaps between frit and top plate. Flow within this gap region could be modeled as two-dimensional flow through porous medium, as case (ii); however, the size and permeability of the gap are unknown.

[1] H. B. van Lengerich, M. J. Vogel, and P. H. Steen, Physica D **238**, 531 (2009).
[2] M. Vogel and P. Steen, Proc. Natl. Acad. Sci. U.S.A. **107**, 3377 (2010).
[3] T. Eisner and D. J. Aneshansley, Proc. Natl. Acad. Sci. U.S.A. **97**, 6568 (2000).
[4] G. Walker and D. Beebe, Lab Chip **2**, 131 (2002).
[5] I. Meyvantsson, J. W. Warrick, S. Hayes, A. Skoien, and D. J. Beebe, Lab Chip **8**, 717 (2008).
[6] J. W. Cahn, Trans. Metall. Soc. AIME **242**, 166 (1968).
[7] D. van der Meer, K. van der Weele, and D. Lohse, J. Stat. Mech.: Theory Exp. (2004), P04004.
[8] D. Painter *et al.*, Appl. Math. Lett. **16**, 375 (2003).
[9] P. Perona and J. Malik, IEEE Trans. Pattern Anal. Mach. Intell. **12**, 629 (1990).
[10] S. H. Strogatz, *Nonlinear Dynamics and Chaos: With Applications to Physics, Biology, Chemistry, and Engineering* (Westview Press, Boulder, CO, 1994).
[11] A. J. Bray, Adv. Phys. **51**, 481 (2002).
[12] L. Ratke and P. W. Voorhees, *Growth and Coarsening* (Springer, New York, 2002).
[13] E. D. Siggia, Phys. Rev. A **20**, 595 (1979).
[14] K. B. Glasner and T. P. Witelski, Phys. Rev. E **67**, 016302 (2003).

[15] U. Thiele, M. G. Velarde, K. Neuffer, M. Bestehorn, and Y. Pomeau, Phys. Rev. E **64**, 061601 (2001).
[16] M. B. Gratton and T. P. Witelski, Phys. Rev. E **77**, 016301 (2008).
[17] J. R. Lister, J. M. Rallison, and S. J. Rees, J. Fluid Mech. **647**, 239 (2010).
[18] D. van der Meer, K. van der Weele, and D. Lohse, Phys. Rev. Lett. **88**, 174302 (2002).
[19] T. Witelski, D. Schaeffer, and M. Shearer, Physica D **160**, 189 (2001).
[20] R. V. Kohn and F. Otto, Commun. Math. Phys. **229**, 375 (2002).
[21] S. Esedoḡlu and D. Slepčev, Nonlinearity **21**, 2759 (2008).
[22] J. Koplik, J. Fluid Mech. **119**, 219 (1982).
[23] J. Van Brakel, Powder Technol. **11**, 205 (1975).
[24] M. B. Gratton and T. P. Witelski, Physica D **238**, 2380 (2009).
[25] I. M. Lifshitz and V. V. Slyozov, J. Phys. Chem. Solids **19**, 35 (1961).
[26] C. Wagner, Ber. Bunsenges. Phys. Chem. **65**, 581 (1961).
[27] L. C. Brown, Acta Metall. **37**, 71 (1989).